Broadband All-Order Polarization Mode Dispersion Compensation Using Liquid-Crystal Modulator Arrays

Mehmetcan Akbulut, *Member, IEEE*, Andrew M. Weiner, *Fellow, IEEE*, and Peter J. Miller

***Abstract*—Polarization mode dispersion (PMD) is a potential limiting factor in long-haul high-speed optical communications, especially in systems beyond 10 Gb/s. Although considerable effort has been devoted to compensation methods for PMD, most of the research is restricted to a small bandwidth, within the limits of the first- and second-order PMD approximations. For the first-order approximation to be valid, the distortions induced by PMD must remain less than a few tenths of the pulse duration or the bit period for return-to-zero (RZ) or non-return-to-zero (NRZ) systems, respectively. In this work, as far as the authors know, the application of ultrafast optical pulse-shaping techniques for experimental broadband all-order PMD compensation is demonstrated for the first time. PMD is treated as arbitrary variations of state of polarization (SOP) and phase versus wavelength, in an all-order sense. Two fiber-pigtailed pulse shapers are implemented in a serial manner to compensate the polarization and phase spectra independently. The first step corrects the wavelength-dependent polarization states to a fixed wavelength-independent state. This reduces the PMD compensation problem to a generalized chromatic dispersion compensation problem. Consequently, equalization of the spectral phase in the second step restores the clean broadband pulse signal. In the experiments, compensation of subpicosecond pulses (14 nm bandwidth around 1550 nm) that are anomalously spread to more than 2 ps due to PMD is demonstrated. These results are potentially relevant for future ultrahigh-speed time-division-multiplexed (TDM) systems. Research challenges that must be addressed to bring this approach to practical application are also briefly enumerated, and the potential for scaling to a range compatible with wavelength-division-multiplexed (WDM) systems is discussed.**

***Index Terms*—All-order PMD compensation, fiber optics communications, liquid-crystal devices, polarization mode dispersion, pulse shaping.**

I. Introduction

POLARIZATION mode dispersion (PMD) is a potential limiting factor in long-haul high-speed optical communications, especially in systems beyond 10 Gb/s [1]. PMD is often categorized in a Taylor series expansion framework in terms of the first-order PMD, second-order PMD, etc. The majority of the research so far is restricted to a small bandwidth, covering the first- and second-order PMDs [1]–[14]. For the first-order PMD approximation to be valid, the distortions induced by PMD must typically remain less than a few tenths of the pulse duration for return-to-zero (RZ) systems [or roughly 10% of the bit period for non-return-to-zero (NRZ) systems]. However, as pulse durations decrease and bandwidths per channel increase, the first-order PMD approximation will become insufficient [1]. For PMD-induced distortions approaching or exceeding the pulse duration, the Taylor series expansion framework becomes inadequate. In this limit, "all-order" PMD must be considered. Some devices potentially suitable for all-order PMD compensation were previously introduced but tested only with first-order PMD emulators [15]. Recently, a few new schemes for all-order PMD compensation and broadband polarization-dependent loss (PDL) compensation have been proposed [16]–[18]. However, most all-order compensator ideas involve a series of birefringent sections or all-pass filters concatenated in a serial fashion. Because the effects of different elements interact in such serial schemes, complex control algorithms are required for arbitrary PMD compensation. These algorithms are still developing and not yet at a practical demonstration stage. In contrast, the PMD compensation scheme that we describe here takes a wavelength-parallel approach, which we believe offers the potential for simpler control algorithms.

Contrary to the Taylor expansion definition of the PMD orders, we choose to view all-order PMD as arbitrary variations of spectral phase and spectral state of polarization (SOP). For the current work, we assume no PDLs or polarization-dependent gains (PDGs) in the system. In order to fix the spectral distortions induced by PMD, in this paper, we demonstrate the application of ultrafast pulse-shaping techniques. Pulse shaping has been proven to be an effective way of implementing arbitrary phase and amplitude filter functions in the past [19], [20] and arbitrary polarization filter functions more recently [21], [22]. For this work, a two-stage compensation scheme that is consistent with our view of PMD is implemented. A "SOP pulse shaper" and a "phase-only pulse shaper" are used in series to independently equalize polarization spectra and phase spectra. This scheme can be used to compensate essentially arbitrary PMD on a frequency-by-frequency basis. Here, we report a detailed discussion of PMD compensation experiments for subpicosecond pulses (14-nm bandwidth centered on the 1550-nm telecommunications band), originally distorted

Manuscript received July 26, 2005; revised October 25, 2005. This work was supported by the National Science Foundation under Grants 0140682-ECS and 0501366-ECS.

M. Akbulut was with the Department of Electrical and Computer Engineering, Purdue University, West Lafayette, IN 47907 USA. He is now with Pritel, Inc., Naperville, IL 60567 USA.

A. M. Weiner is with the Department of Electrical and Computer Engineering, Purdue University, West Lafayette, IN 47907 USA (e-mail: amw@ecn.purdue.edu).

P. J. Miller is with Cri-Inc., Woburn, MA 01801 USA.

Digital Object Identifier 10.1109/JLT.2005.861143

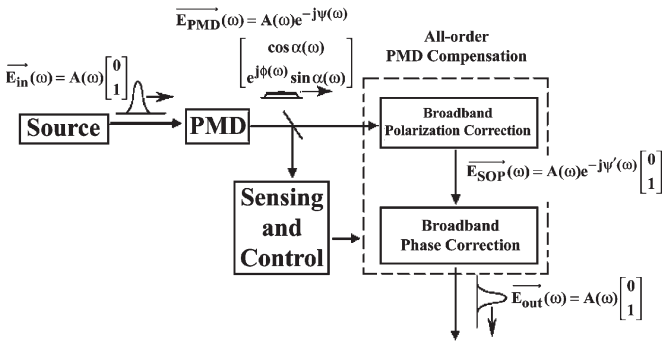

Fig. 1. All-order PMD compensation in feedforward configuration. Simplified equations are inserted at each step to clarify. Detailed equations can be found in Section II.

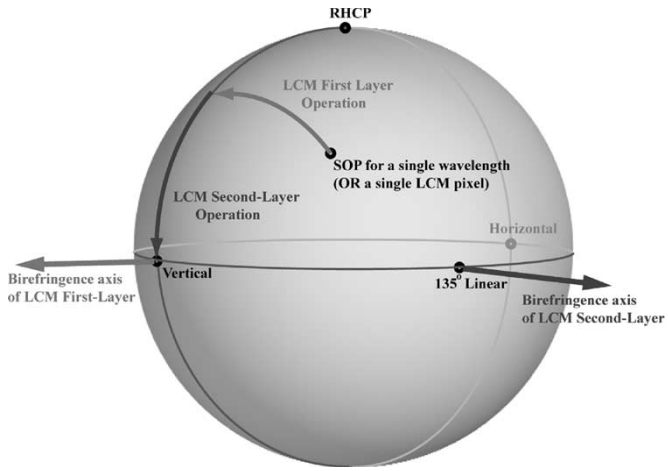

Fig. 2. SOP correction illustration.

to a duration of more than 2 ps (several pulsewidths), from which the original pulse was successfully recovered. A short description of this work is published elsewhere [23], [24]. To our knowledge, our results constitute the first proof-of-concept demonstration of a PMD compensator based on an optical pulse-shaping scheme and the first experimental demonstration of all-order PMD correction for subpicosecond pulses.

Our scheme implements simple feedforward control algorithms (Fig. 1). The basic idea here is to measure the spectral SOP and spectral phase information, calculate the necessary frequency-dependent polarization and phase filter functions, and apply them with the pulse shapers. Furthermore, this two-step approach gives us the choice to equalize only polarization (eliminates PDL/PDG in subsequent components), only phase (equivalent to all-order chromatic dispersion compensation), or both (full PMD compensation). Furthermore, if we were to upgrade the phase-only pulse shaper to a "phase/amplitude" pulse shaper, we can even equalize the PDL/PDG in the system.

The remainder of this paper is structured as follows. Section II covers the theoretical underpinnings of our approach, including details on the liquid-crystal modulator (LCM) elements used in the pulse shapers, simulation results, and discussion on the boundaries of first-order and all-order PMD regimes. Section III covers the experimental setup. Section IV describes the approach used in our experiments to estimate the spectral phase needed for the final stage of PMD compensation. Experimental results are presented in Section V. Section VI summarizes and discusses some of the challenges needed to further our laboratory proof-of-concept experiments to a practical compensator for real-world applications.

II. Theory

In this section, we will introduce our broadband PMD compensation technique in two steps, namely 1) broadband polarization correction and 2) broadband phase correction. This scheme has the potential to compensate subsequent PDL effects in the first step, and to compensate for all-order PMD on the overall. PDL compensation comes naturally from aligning all the wavelengths to the same linear SOP, thus, handling the polarization effects of subsequent elements in the optical network. We will also present some simulation results and a theoretical discussion on the all-order PMD bandwidth for NRZ and RZ systems.

A. Pulse Shaping and PMD

The key technology in our experiments is the ultrafast pulse-shaping apparatus pioneered by Weiner [19]. The apparatus consists of a wavelength disperser element (usually a grating), imaging elements (lenses), and a programmable LCM array to manipulate the amplitude and/or phase of each wavelength individually. It can be thought of as a fully adjustable amplitude/phase filter for optical beams, in analogy with programmable electronic filters that are used in nonoptical systems. In the current experiments, we implement each of the pulse shapers in a double-pass geometry using a retroreflecting mirror after the LCM, which reduces the component count and saves space.

Next, we extend the amplitude and phase control to polarization control. To accomplish the polarization correction task, we have designed a two-layer LCM array that can rotate any arbitrary input polarization state to a fixed $\boldsymbol{x}$ or $\boldsymbol{y}$ state on a wavelength-by-wavelength fashion [21], [25]. The device consists of 128 pixels for each layer at 100-μm spacing, and each pixel of each layer provides individual retardation control in the range $[\pi, 3\pi]$. The geometry is given as follows: The voltage-controlled axis of the first layer is at 90° ($\boldsymbol{y}$-axis), and the second layer is at 45°. Using measurement data of the input polarization spectrum and a simple algorithm, we program the LCM to rotate all the frequencies to align with the $\boldsymbol{y}$-axis. The first layer rotates the input SOP on the Poincaré sphere around the S_1 axis to a point on the great circle that goes through the poles and vertical/horizontal polarizations. Then, the second layer rotates around the S_2 axis to the destination point (see illustration in Fig. 2). Individually carrying out these rotations for the 128 pixels enables to correct the SOP for each frequency component.

Following this polarization operation, an additional one-layer LCM at 90° ($\boldsymbol{y}$) is used in pure phase mode to correct the remaining frequency-dependent phases (or delays). This is equivalent to generalized all-order chromatic dispersion compensation. All of these three LCM array layers can potentially

be incorporated into a single package, simplifying the setup and reducing losses associated with coupling light from one setup to the other. It is worth mentioning that our proposed 90°–45°–90° liquid-crystal orientation has been used for arbitrary polarization rotation previously [26], but the idea there is to rotate any arbitrary input polarization state to a desired arbitrary output state. In addition, those devices work in a single pixel (serial) fashion and are not intended for PMD.

To go over the equations for the PMD equalization algorithm, we will assume the wavelength-dependent electric field Jones matrices for the input signal (from the laser) $\overrightarrow{E_{\text{in}}}$ and the PMD distorted signal $\overrightarrow{E}(\omega)$ as

$$\overrightarrow{E_{\text{in}}} = A(\omega)\begin{bmatrix}\cos\,\delta\\ e^{j\chi}\,\sin\,\delta\end{bmatrix}$$

$$\overrightarrow{E}(\omega) = A(\omega)e^{-j\psi(\omega)}\begin{bmatrix}\cos\,\alpha(\omega)\\ e^{j\phi(\omega)}\,\sin\,\alpha(\omega)\end{bmatrix} \tag{1}$$

where $A(\omega)$ denotes the power spectrum. The input signal polarization and power spectrum do not need to be known, and the first equation above just emphasizes that the polarization, and phase are not a function of wavelength before the PMD effects. For now, let us assume that the PMD distorted electric field information is known. Our experimental approach, which uses wavelength-parallel polarimetry to obtain $\alpha(\omega)$ and $\phi(\omega)$, and phase retrieval to obtain $\psi(\omega)$, is described in Sections III and IV, respectively. If the phase retardation through the layers of the LCM array is $\theta_{1,2}(\omega)$ (for layers 1 and 2), where the ω dimension is covered by the different pixels of the array, then we can write the transfer matrices of the two layers as

$$T_1(\omega) = e^{jK_1}\begin{bmatrix}1 & 0\\ 0 & e^{j\theta_1(\omega)}\end{bmatrix}$$

$$T_2(\omega) = S\left(\frac{\pi}{4}\right)e^{jK_2}\begin{bmatrix}1 & 0\\ 0 & e^{j\theta_2(\omega)}\end{bmatrix}S\left(-\frac{\pi}{4}\right)$$

$$\begin{aligned}T_{\text{total}}(\omega) &= T_2(\omega)T_1(\omega)\\ &= e^{j\left(\frac{\theta_2(\omega)}{2}+K_1+K_2\right)}\\ &\quad\times\begin{bmatrix}\cos\left(\frac{\theta_2(\omega)}{2}\right) & j\sin\left(\frac{\theta_2(\omega)}{2}\right)e^{j\theta_1(\omega)}\\ j\sin\left(\frac{\theta_2(\omega)}{2}\right) & \cos\left(\frac{\theta_2(\omega)}{2}\right)e^{j\theta_1(\omega)}\end{bmatrix}\end{aligned} \tag{2}$$

where $S(\text{angle})$ is the standard Jones matrix for reference frame rotation and K_1 and K_2 are constant phase factors. Consequently, the output of the two-layer polarization compensator is given by (3), shown at the bottom of the page. In order to set the polarization spectrum to $\boldsymbol{y}$ linear state at every wavelength (with the final result of polarization compensation), we choose the phase retardation parameters as

$$\begin{aligned}\theta_1(\omega) &= \frac{\pi}{2} - \phi(\omega)\\ \theta_2(\omega) &= \pi - 2\alpha(\omega)\\ \overrightarrow{E_{\text{two-layer out}}}(\omega) &= A(\omega)e^{-j\psi(\omega)}e^{j(K_1+K_2+\pi-\alpha(\omega))}\begin{bmatrix}0\\1\end{bmatrix}.\end{aligned} \tag{4}$$

Basically, by adjusting $\theta_{1,2}(\omega)$, it is possible to rotate from an arbitrary point of the Poincaré sphere to any point on the great circle (which goes through horizontal, vertical, and circular polarizations) and beyond (with limitations). The equations in this section present the $\boldsymbol{y}$ linear state, and in our experiments, we chose to rotate to either $\boldsymbol{x}$ or $\boldsymbol{y}$.

The equations above are presented for the standard single-pass pulse shaper setup with two LCM layers. For a double-pass pulse shaper, we need some modifications to the matrices and the required phase retardations. Basically, the phase retardation of the second layer (voltage axis at 45°, closest to the mirror) has to be halved from what it was before. In this new scheme, after passing through the two layers, the mirror and the second layer again, the wavelengths are arranged to be rotated to $\boldsymbol{y}$ polarization, so the passage through the first layer (voltage axis at 90°) only introduces an additional spectral phase that is known (with no further polarization rotation). The electric field after SOP compensation is

$$\begin{aligned}&\overrightarrow{E_{\text{two-layer out}}}(\omega)\\ &\quad= A(\omega)e^{-j\psi(\omega)}e^{j\left[2(K_1+K_2)+\frac{3\pi}{2}\alpha(\omega)-\phi(\omega)\right]}\begin{bmatrix}0\\1\end{bmatrix}.\end{aligned} \tag{5}$$

It is visible that, compared to (4), the double-pass compensated signal has one more spectral phase term; however, this term is already known, and it factors into the phase compensation easily. In each case, there is still a frequency-dependent phase, arising from the polarization terms $\alpha(\omega)$ and $\phi(\omega)$, which are known from the polarimetry, and the phase factor $\psi(\omega)$, which is not. The job of the phase-only compensator will be to equalize out this remaining phase, after which all of the PMD effects will be gone.

B. Simulation Results

We have carried out simulations of the proposed scheme with 800-fs [intensity full-width at half-maximum (FWHM)] pulses. The model in the simulation consisted of 5000 identical waveplates, each with differential group delay (DGD) of 0.046 ps (for a 3-ps mean DGD simulation) or 0.307 ps (for a

$$\begin{aligned}\overrightarrow{E_{\text{two-layer out}}}(\omega) &= T_{\text{total}}(\omega)\overrightarrow{E}(\omega)\\ &= A(\omega)e^{-j\psi(\omega)}e^{j\left(\frac{\theta_2(\omega)}{2}+K_1+K_2\right)}\begin{bmatrix}\cos\,\alpha(\omega)\cos\left(\frac{\theta_2(\omega)}{2}\right)+j\,\sin\,\alpha(\omega)\sin\left(\frac{\theta_2(\omega)}{2}\right) & e^{j\phi(\omega)}e^{j\theta_1(\omega)}\\ j\,\cos\,\alpha(\omega)\sin\left(\frac{\theta_2(\omega)}{2}\right)+\sin\,\alpha(\omega)\cos\left(\frac{\theta_2(\omega)}{2}\right) & e^{j\phi(\omega)}e^{j\theta_1(\omega)}\end{bmatrix}\end{aligned} \tag{3}$$

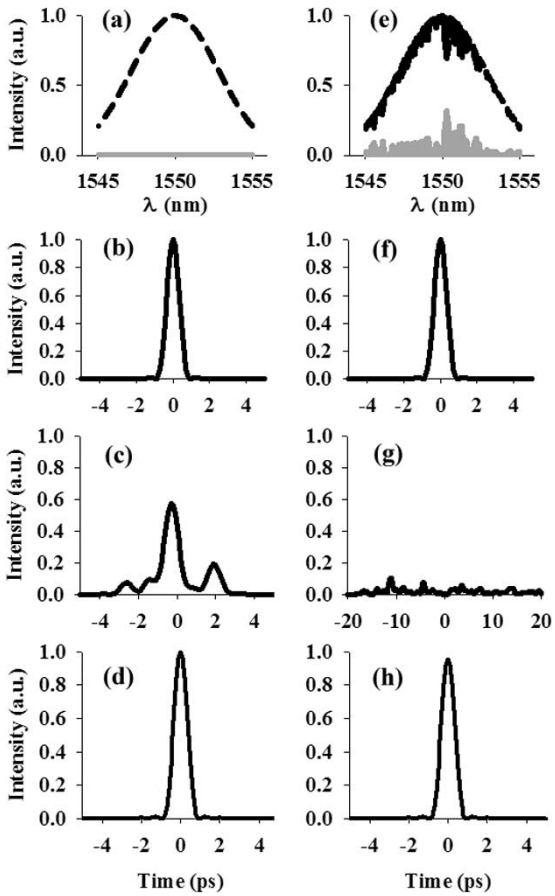

Fig. 3. Simulation for mean DGD of (a)–(d) 3 ps and (e)–(f) 20 ps. Top row: power spectrum for $\boldsymbol{x}$ (light) and $\boldsymbol{y}$ (dark) polarizations after PMD compensation. Second row: input pulse. Third row: time-domain waveforms after PMD effects. Fourth row: time-domain waveforms after PMD compensation.

20-ps mean DGD simulation), with random birefringence axis orientations. This method of simulation is known to give good statistical probability distributions [27]. The drawback of this design is that it will have a periodic structure that scales with the inverse of the DGD of a single waveplate. These periods are calculated as 173.9 and 26 nm for the 3- and 20-ps mean DGD, respectively, which exceeds the 10-nm bandwidth around 1550 nm used in the simulations.

In Fig. 3, we show the compensation results for the above cases of mean DGD. There are 128 pixels on the LCM with each pixel covering 0.078 nm (10 nm total bandwidth). Although the simulations show highly complex pulses for both 3- and 20-ps mean DGD, in both cases, after compensation, the pulses are restored cleanly to the original 800-fs duration. In the 20-ps mean DGD case, after compensation, the $\boldsymbol{x}$ and $\boldsymbol{y}$ polarized spectra exhibit structure, which shows that the compensator is unable to fully restore the field to a single linear polarization state. With increasing DGD, the PMD-induced polarization and phase variations increase rapidly with frequency. Structure such as that shown in the 20-ps simulation occurs when the pixel size of the LCM array is not fine enough to adequately sample the rapid PMD fluctuations. In fact, this aliasing concept is related to the issue of finite spectral resolution in optical pulse shaping [19], [28]–[31], which generally applies for pixilated as well as nonpixilated spatial light modulators. The main point is that the spectral variation across neighboring pixels has to be small in order to avoid diffraction at the edges of the pixels; hence, the spectral function applied via the LCM array should be smooth. The analysis on pixilation and finite spectral resolution limits in the pulse shaping literature (for phase and amplitude pulse shaping) is directly extendable to the case of polarization and phase pulse shaping considered here.

Directly related to the aliasing is the maximum amount of PMD that can be compensated (or emulated). This is mainly determined by the frequency width δf of one LCM pixel. In order to avoid aliasing at the LCM array, spectral variations should be slow compared to this frequency width. It has been shown that this requirement is equivalent to having a signal with a time aperture of much less than $1/2\delta f$ [30]. For the simulation above, δf is 9.76 GHz. Thus, for high-quality compensation, the PMD-distorted signal should occupy a time aperture much less than 51 ps. This is roughly in agreement with the simulation results (departure from ideal operation is beginning to be seen for the 20-ps mean DGD, though good compensation is still achieved). The PMD compensator can be designed to handle different time duration specifications by varying δf through choice of optical elements.

In order to more clearly establish the amount of PMD that can be compensated with our approach, in future work, one could analyze how the compensated waveforms degrade as a function of the rate of polarization and phase change at the input to the compensator, relative to pulse shaper spectral resolution and pixel spacing δf. One can then envision applying statistical measures of PMD worked out in the literature in order to estimate system outage probability as a function of mean DGD. However, this analysis is beyond the scope of our current work, in which the focus is on proof-of-concept experimental demonstration.

C. All-Order PMD Bandwidth

Building on the first-order PMD bandwidth formula [1], bandwidth of higher-order PMD was recently investigated [32]. From this formulation, the bandwidth Δf_{PSP} for the first, second, third, fourth, 12th and 19th orders of 1-ps mean DGD were given as 125, 258, 336, 392, 632, and 764 GHz, respectively [32]. Thus, the PMD bandwidth for the nineteenth order, which can be considered as an approximation to all orders, happens to be 6.12 times the bandwidth for first-order PMD.

In a pulsed system (RZ), one would also like to calculate the minimum pulsewidth to remain in the first-order PMD regime. For a transform-limited Gaussian shape for the pulse, taking the $1/e^2$ bandwidth equal to the first-order bandwidth of the PMD vector, the FWHM pulsewidth scales with the mean DGD as

$$\Delta t_{\mathrm{FWHM}} = 6\langle \Delta\tau \rangle. \tag{6}$$

Thus, for a 1-ps mean DGD fiber, the RZ pulse has to be larger than 6 ps in FWHM in order to be considered in the first-order regime. Allowing a generic 50% RZ duty cycle, the bit period is obtained as 12 ps, which gives the maximum bit rate of 83 Gb/s for first-order PMD regime. It can be noted that, using

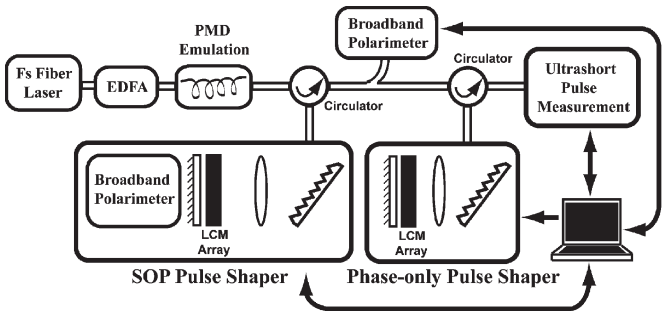

Fig. 4. Full experiment setup.

the earlier definitions, the pulse needs to be larger than 980 fs in FWHM to remain in the nineteenth order of PMD for this case. Thus, if we use the 19th-order bandwidth as a criterion for crossing into the all-order PMD domain, we find that when the mean DGD is greater than or equal to the time-domain intensity FWHM, for a Gaussian pulse, the system should be considered in the all-order PMD regime. Since our simulations assumed 800-fs pulses, with mean DGDs of 3 and 20 ps, respectively, the simulations were clearly in the all-order PMD regime.

III. Experiment Setup

The full PMD compensation experiment setup is shown in Fig. 4. The light source is a passively mode-locked femtosecond fiber laser centered in the 1550-nm region, and the pulsewidth estimated from autocorrelation is 72 fs (intensity FWHM). Some of the power from the laser output is tapped and connected to the reference arm of the cross correlator in the experiment setup (ultrashort pulse measurement). The remaining signal is filtered to the 1542–1556 nm region and amplified with the erbium-doped fiber amplifier (EDFA) to be used in the PMD compensation experiments. The resulting input pulsewidth to the experiment setup is measured to be as low as 576 fs (best chromatic dispersion compensated case). The PMD emulator consists of various numbers of polarization-maintaining (PM) fiber sections with different lengths and concatenation angles. The details will be mentioned in Section V. In what follows, we explain the setup in two stages, describing first the broadband SOP equalizer (SOP pulse shaper) and then the broadband phase equalizer (phase-only pulse shaper).

A. Broadband SOP Equalizer

The first part of the SOP pulse shaper consists of a fiber collimator with $1/e^2$ intensity beam width of 1.9 mm, magnified by a 3.55$\times$ beam expander. The expanded beam diffracts off a low-PDL grating with 600 lines/mm features and is focused with an achromatic doublet (achromat) imaging lens with 300 mm focal length. At this point, there is another 3.55$\times$ beam expander. The function of the beam expanders is to fill the entire LCM array aperture with good spectral resolution per pixel size and with some reduction in overall length of the setup. The grating is required to be low PDL, since the SOP versus wavelength at this point will be distorted due to PMD. The size of the grating is 1 $\times$ 1 in and it was experimentally found to have $\sim$ 0.02 dB PDL at an incident angle of 12.4°. Using this incident angle of 12.4°, the diffraction angle is calculated as 45.74°, and the beam size at the LCM array image plane is measured as 154 μm (intensity FWHM). A partial reflective mirror is placed after the LCM for double passing through the setup. Of course, a low-PDL optical circulator is required in this case to separate the input and output beams in the fiber. In the current setup, which uses a number of extra lenses not used in our standard reflective pulse shapers, the double-pass power loss was measured as low as 7.63 dB. The loss numbers for the grating and the circulator are 3 dB (double pass) and 2 dB (input port to output port); $\sim$ 1 dB loss from the LCM array, 0.46 dB loss from the partial reflective mirror (90% reflective), and the remaining 1.13 dB from misalignments or reflections at lens surfaces add up to 7.63 dB total loss number. The reason for the partial reflectivity of the mirror is the SOP measurement apparatus discussed below.

One difficulty with the double-pass pulse shaper is that the wavelengths are now focused at the mirror plane instead of the LCM pixels. This reduces the available spectral resolution at the LCM plane and, thus, degrades the performance. For the LCM array used in the current experiments, the design of the mechanical case places the LCM pixels approximately 19 mm away from the turnaround mirror. Consequently, the beam size at the LCM is increased to approximately 268 μm. With a redesigned mechanical case, available now but not at the time of our experiments, single pixel resolution can be retained even in the double-pass geometry [33]

1) Broadband Polarization Measurement: In parallel to the PMD compensation work, we have been pursuing a broadband polarimeter project. This project was initiated to satisfy the measurement of the wavelength-dependent SOP in parallel, which is required for the fast operation of the SOP correction algorithm. At the time, there were no commercial wavelength-parallel broadband polarization measurement apparatus available—this continues to be the case today. The key technology here is fast-switching ferroelectric liquid crystals (FLCs) for sequential polarization selection, and the use of a grating and detector array camera to measure all the wavelengths in parallel. This polarimeter has the ability to measure 256 wavelengths in parallel, potentially within 1 ms [34].

The placement of this polarimeter in the SOP pulse shaper requires care. One concern is that due to slight polarization changes at the grating, either the wavelength-dependent polarization matrix of the grating must be calibrated for polarization sensing before the grating, or the SOP must be sensed after the grating. An innovative solution we found was to place the broadband polarimeter behind the return mirror of the double-pass SOP pulse shaper (Fig. 5). This way, we can measure the polarization without disturbing the signal and the SOP correction process, and, also, we can reduce the elements in the polarimeter, since the wavelengths are already dispersed in the SOP pulse shaper. Assuming a partially reflective mirror will not change the polarization states of the incoming wavelengths (which holds due to the normal incidence of the light on the mirror), and that we set the LCM array to be inactive (i.e., 2π phase retardation), we can get a reliable measurement of SOP versus λ by this scheme. The wavelengths are transferred to the camera plane from the mirror plane by a one-to-one

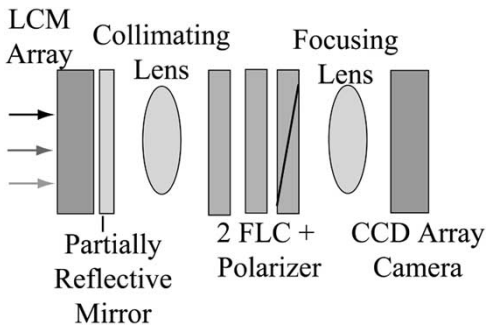

Fig. 5. Broadband polarimeter inside the SOP pulse shaper.

imaging system with two 10-cm lenses. The reflectivity of the mirror was 90%, and the remaining light was enough to get good SNR from the camera readout. The resolution at the camera plane was measured to be 150 μm. This is similar to the resolution at the partially reflective mirror plane. In a real-time telecommunication system, the polarization data will have to be continuously read and compensated. In this case, the measured SOP data could be inverted in order to obtain the original polarization states prior to the LCM. This is easily accomplished by using the known calibration of LCM polarization transformation versus pixel settings.

We needed another broadband polarimeter at the output of the SOP pulse shaper to check the quality of SOP correction. Consequently, we constructed a second FLC polarimeter. This time, we used a conventional optical spectrum analyzer (OSA) to replace the grating and the camera to generate a very simple broadband serial polarimeter. It is slower than the parallel polarimeter we built inside the pulse shaper (due to the OSA scan speed) but is more sensitive. Ten percent of the light is tapped from the output of the SOP pulse shaper for this broadband polarimeter, and the remaining power goes into the "phase-only" pulse shaper. The finalized broadband polarization equalizer setup is shown in Fig. 6.

B. Broadband Phase Equalizer

Following on the same lines as the SOP pulse shaper, a double-pass phase-only pulse shaper is needed to equalize the spectral phase from PMD, plus the introduced phase from the SOP LCM array. The inherent quadratic and cubic chromatic dispersion in the whole setup due to the single mode fibers were compensated with an optimized length of dispersion-compensating fiber that also approximately matches the dispersion slope of the single mode fiber (SMF). Thus, the PMD compensator would not have to worry about the static chromatic dispersion in the system, and would only work on correcting the PMD effects. The design of the phase-only pulse shaper is much simpler than the SOP pulse shaper, since we can assume that the input polarization spectrum is already equalized to a fixed linear polarization. Thus, we do not need to have a low-PDL grating, and this opens up the possibility of using a high groove density grating with large input angles to increase spectral dispersion and to reduce the number of lenses. We used a 2 $\times$ 2 in 1200 lines/mm grating with $\sim$ 90.2% absolute first-order diffraction efficiency with $\boldsymbol{x}$ polarization.

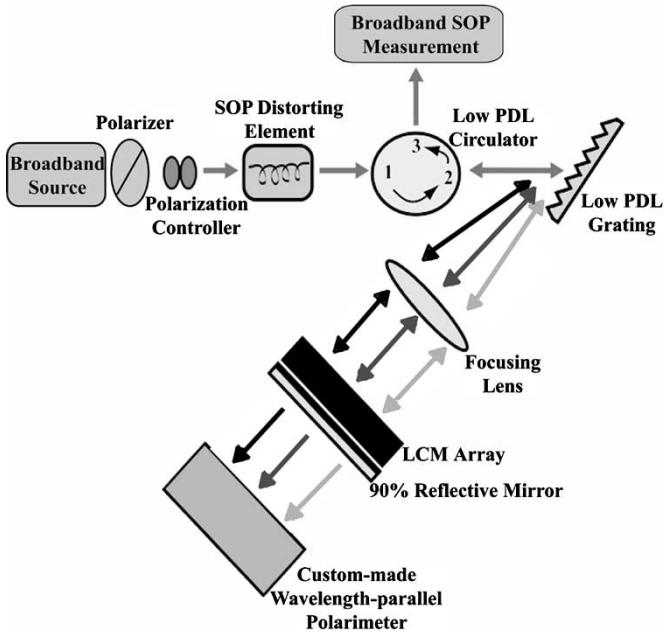

Fig. 6. Broadband polarization equalizer setup.

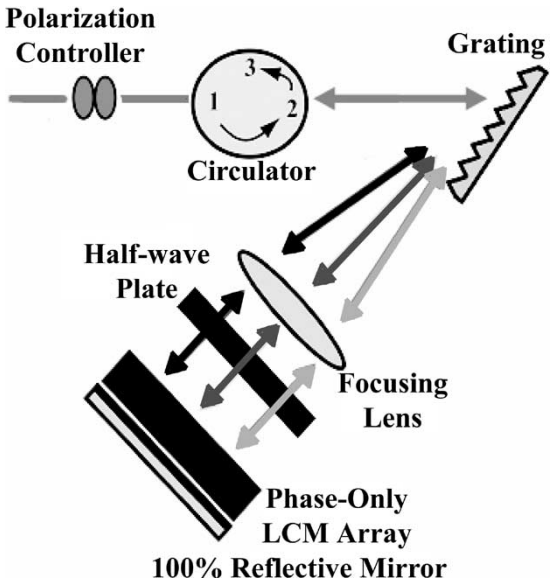

Fig. 7. Broadband phase equalizer setup.

A polarization controller is required before the setup to match the polarization of the SOP-corrected signal to the $\boldsymbol{x}$-axis of the grating. We use a 70° incidence angle, which gives $\sim$ 67° as the diffraction angle. Although a 300-mm focal length achromat is used as the imaging lens as in the SOP pulse shaper, the beam expanders are not necessary in this case due to high resolution of the pulse shaper and the use of a 2.7-mm beam size collimator at the input. The resolution at the LCM array image plane was measured as 98 μm. This is very close to one LCM pixel per wavelength, which is good enough for our purposes. The final setup is shown in Fig. 7. The half-wave plate is used to rotate the horizontal polarization coming from the grating to the vertical polarization that is required by the single-layer LCM used for phase-only control in our setup.

The insertion loss of this pulse shaper is $\sim$ 4.5 dB including the circulator.

IV. Spectral Phase Retrieval Problem

In all the LCM phase calculations of Section II, we were assuming one thing—that we have measured the frequency-dependent common mode phase $\psi(\omega)$. Instead, determination of this phase is a nontrivial task. In principle, methods for complete amplitude and phase characterization of ultrashort pulses, such as frequency-resolved optical gating [35], can be used to obtain the spectral phase. However, the setup is relatively complex, and such methods may encounter difficulty in the case of waveforms of the complexity considered here. Thus, for the experiments reported here, we decided to make use of the well-known "Gerchberg–Saxton (GS) algorithm" [36], [37]. This algorithm only requires knowledge of the time- and frequency-domain intensities, and, in theory, the convergence is unique. In the experiments, we measure the time-domain intensity using an intensity cross correlator. Considering that we deal with PMD-distorted waveforms on the order of picoseconds or above, using the 72-fs reference pulse in the cross correlation measurement is similar to using a delta function. Thus, we could get a very good approximation of the time-domain intensity. The phase retrieval process starts with an initial spectral phase guess (which was zero in our case) and usually converges rapidly (typically 70–250 iterations needed in our case). We used the MATLAB environment for the phase retrieval calculations, with convergence typically on the order of seconds. This time can be reduced quite significantly in a real-world application by the use of dedicated signal processing hardware.

In practice, our experimental results using the GS algorithm for phase sensing were not as clean as desired. Referring, for example, to Fig. 10, a series of side lobes accompany the compensated pulse, most likely due to inaccuracies in the phase estimate. Such imperfect compensation might also arise due to finite resolution of the SOP and phase-only pulse shapers, which limit the amount of PMD fluctuations that can be compensated. In order to improve, we decided to run an iterated version of the GS algorithm. The algorithm is run once with the time- and frequency-domain measurements, and the retrieved phase is applied to the phase-only LCM array. Then, the resultant time-domain waveform is measured and used as the starting point for another GS phase retrieval problem, with the original power spectrum from the OSA. The output of this new run gives a correction factor to the initially estimated phase. With this strategy, the complexity of the waveform to be retrieved should decrease in increasing iterations. This is expected to be helpful, since the GS algorithm has no mechanism for correcting inaccuracies in the measured time- and frequency-domain waveform inputs into the algorithm. This iterated GS algorithm should allow more accurate phase retrieval while also compensating in part for inaccuracies in the phase calibration of the LCM. The sign of the correction was decided manually, based on which sign gives a cleaner time-domain waveform. This iterated GS algorithm gave us significantly cleaner pulses, usually in less than seven iterations (see the example in Fig. 8).

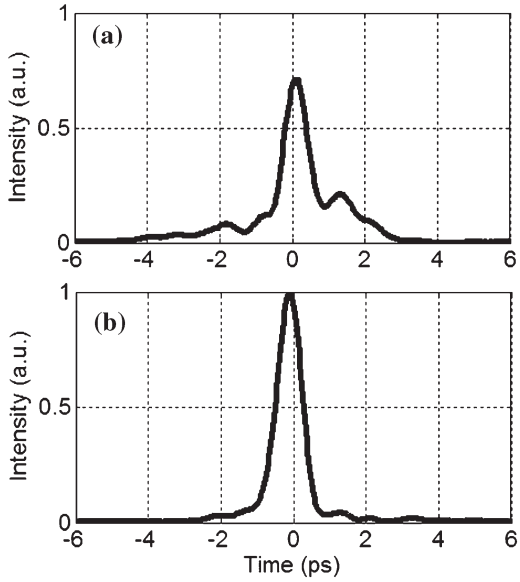

Fig. 8. Time-domain waveform comparison for iterated GS algorithm. (a) For one iteration. (b) For six iterations.

In most cases, the signs of the consecutive phase correction factors turned out to be alternating.

This phase-sensing scheme sufficed for our laboratory demonstrations of all-order PMD compensation reported in the next section. It is clear, however, that for practical applications, further research is required to identify a better and more robust phase-sensing scheme.

V. Experimental Results

Our experiments are performed using a "PMD emulator" consisting of one or two segments of "eight-piece PM fiber" concatenations. This element introduces the PMD-like behavior of wavelength-dependent polarization states and phases, which we will then correct for. There are spliced SMF pigtail connectors after each eight-piece PM fiber segment, which introduce additional polarization rotation between the segments. In order to obtain different PMD distortions for our experiments, we either use the polarization controller prior to the PM fiber segments or change the order of the eight-piece segments. Considering the estimated mean DGD values of 722 fs and 1.29 and 1.38 ps for the different experiment trials, the emulation can be considered as all-order PMD according to the discussion in Section II. The input pulsewidths for the different PMD compensation examples range from 576 to 792 fs due to differences in the accuracy of chromatic dispersion compensation.

The step-by-step procedure for PMD compensation is displayed in Fig. 9. First, the SOP versus wavelength and time-domain pulse distortions are measured while setting the pulse shapers to be inactive. Then, the appropriate correction algorithm is applied to the SOP pulse shaper to have a single polarization state at the input of the phase pulse shaper. The broadband polarimeter is used at this point to confirm this expectation. Next, the time-domain intensity profile and the optical power spectrum are measured for the Gerchberg–Saxton algorithm. Following that, the phase pulse shaper is

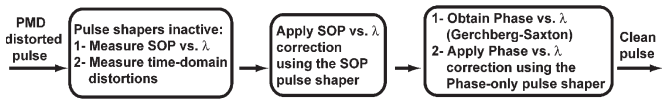

Fig. 9. Step-by-step procedures for full PMD compensation experiment.

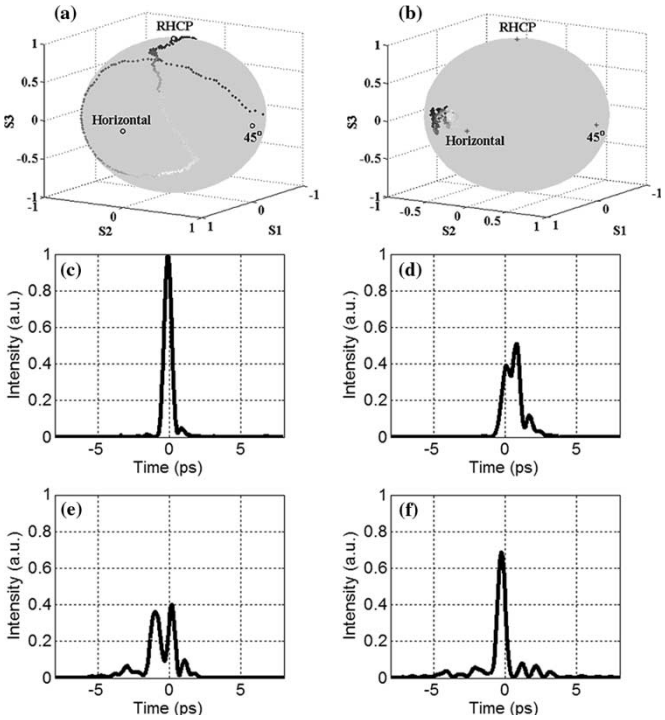

Fig. 10. One eight-piece PM fiber as PMD emulator (mean DGD of 721 fs). Top row: SOP versus wavelength (a) before and (b) after compensation. Middle and the bottom rows: time-domain waveforms (c) at the input, (d) after the PMD emulator, (e) after SOP correction, and (f) after SOP + phase correction.

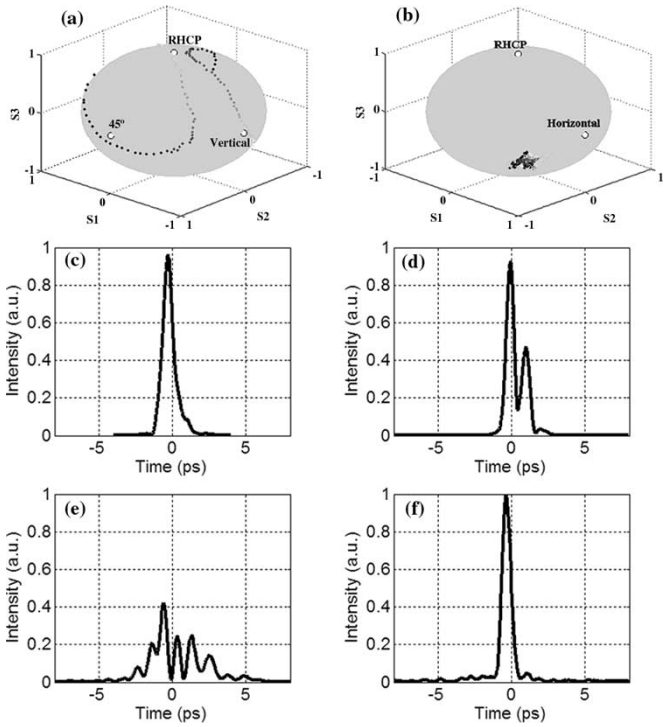

Fig. 11. Two eight-piece PM fiber segments in series as PMD emulator (mean DGD of $\sim$ 1.38 ps), iterated GS algorithm. Top row: SOP versus wavelength (a) before and (b) after compensation. Middle and the bottom rows: time-domain waveforms (c) at the input, (d) after the PMD emulator, (e) after SOP correction, and (f) after SOP + phase correction.

programmed to equalize the remaining spectral phase, and the resulting time-domain intensity is measured again using the cross correlator. In some cases, iteration of the GS algorithm is required, and this measured time-domain waveform is fed back to the GS optimization algorithm. Finally, the outcome is a clean restored femtosecond pulse, with pulsewidth on the order of the input pulse. It is important to note that the whole setup is fiber based, except the two pulse shapers that are free space but fiber coupled.

For purposes of comparison, we also measured the distorted time-domain waveforms prior to SOP equalization, although these data are not required for compensation. Because at this point, the distorted signal has strong SOP versus wavelength variation, and because the cross correlation measurement is based on a polarization-sensitive second harmonic generation interaction, we chose to use the correlator to measure two orthogonal polarization states of the incoming signal. These two cross correlation traces were then added in the software to yield the overall intensity versus time waveform.

The figures are organized such that the top row displays the broadband SOP correction stage, whereas the middle and the bottom rows present the time-domain waveforms before and after each compensation stage. All of the shown polarization measurements are conducted at the output of the SOP pulse shaper. Fig. 10 illustrates a trial with the "eight-piece PM fiber" PMD element with average DGD estimated at 722 fs. Before PMD compensation, the pulse is anomalously spread to a duration of more than 1 ps, with polarization versus wavelength varying dramatically. However, after compensation, it is restored to mostly a single polarization and the FWHM duration is reduced to an FWHM of 627 fs—almost the input pulsewidth of 602 fs.

It is worth noting that the measured time-domain waveforms after SOP correction are more dispersed than before SOP correction. This is expected, because the SOP pulse shaper not only equalizes polarization, but also unavoidably introduces additional spectral phase to the system [see (5) in Section II]. Most of time, this ends up spreading the time-domain waveforms even more. There are some satellites in the time domain that could not be corrected perfectly in this first example, most probably due to the inaccuracies in the phase estimate. This issue is fixed in consequent examples by the iterated GS algorithm.

Fig. 11 demonstrates a trial with the 1.38-ps mean DGD PMD emulator consisting of two eight-piece PM fiber segments and using the GS algorithm iteratively. The input pulsewidth is 792 fs, which is spread to a duration of more than 2 ps after the emulator, with polarization versus wavelength varying dramatically. After PMD compensation, the pulse is restored almost to a single polarization, and the FWHM duration is reduced to 696 fs. The restored pulsewidth is shorter than the input pulsewidth, because the phase pulse shaper also corrected some of the residual chromatic dispersion in the system.

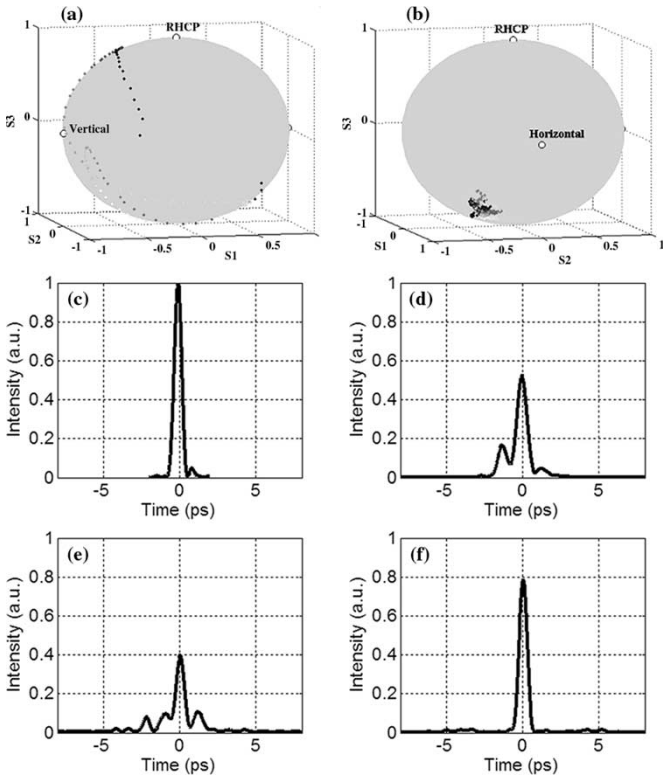

Fig. 12. Two eight-piece PM fiber segments, different ordering of segments (mean DGD of $\sim$ 1.29 ps), iterated GS algorithm. Top row: SOP versus wavelength (a) before and (b) after compensation. Middle and the bottom rows: time-domain waveforms (c) at the input, (d) after the PMD emulator, (e) after SOP correction, and (f) after SOP + phase correction.

In order to observe a different pulse-distortion trial, we reversed the segments of the two eight-piece PM fiber segments (average DGD estimated at 1.29 ps), adjusted the input polarization controller to these segments, and used an input pulse that is compressed to 576 fs (almost transform limited). After compensation, the PMD-distorted pulse was restored to 631 fs, which is roughly the original duration, and the polarization spectrum was again equalized (Fig. 12). In all of these examples, although the time-domain waveform is severely distorted (especially after SOP correction), our PMD compensation apparatus recovers the input pulse fully.

VI. Discussion and Summary

Our experiments demonstrate that by adopting a pulse-shaping approach, one can compensate for strong distortions encountered by subpicosecond pulses due to PMD in the all-order regime. The wavelength-parallel nature of the compensator should aid in the development of relatively simple control algorithms, which can operate directly in the spectral domain, in part based on polarimetry data. However, significant further research is needed to bring this approach to a stage suitable for practical application. Three key points are included.

1) In the research reported here, the PMD is held constant during the course of the experiments. In real systems, dynamic PMD fluctuations must be considered. Our setup is limited primarily by the response time of the LCM arrays. Response times of tens of milliseconds are typical, although some authors anticipate scaling down to a few milliseconds [38]. If achieved, this would bring the response time close to approximately the 1-ms range, which is usually viewed as the target for real-time PMD compensation. Possibly other modulator array technologies faster than liquid crystals can also be developed for this purpose. Finally, for continuous PMD tracking and compensation, endless polarization and phase control will be required (no resets). This will require modulator arrays with at least one more layer than what is considered here, although this has not been addressed in our work to date.
2) As mentioned in Section IV, an improved phase-sensing scheme is needed. In particular, the scheme must work fully automatically and needs to be sufficiently robust for reliable operation. Furthermore, the phase sensing must operate at a speed fast enough to support the desired speed of the overall compensator.
3) As discussed in Section II-B, the amount of PMD (mean DGD) that can be compensated in our approach depends on the spectral resolution of the pulse shapers, the number of control pixels in the modulator array, and the frequency spread per pixel. For systems work, it will be important to establish estimates of outage probability as a function of mean DGD and pulse shaper parameters.

In addition to the specific scheme adopted here, namely spectral SOP equalization followed by spectral phase compensation, our pulse-shaping approach can be generalized to implement other schemes operating in the spectral domain. This may provide the opportunity to optimize the overall system operation, including both physical compensation and sensing and control. For example, Phua *et al.* [16] propose and analyze all-order PMD compensation based on direct manipulation of the frequency-dependent PMD vector. The SOP pulse shaper demonstrated in our work can, in principle, be programmed to provide a frequency-independent alignment direction for all the PMD vectors, proposed as the first stage of compensation in [16], while phase pulse shaping can be extended to provide the frequency-dependent differential group delay then needed to cancel the aligned PMD vectors (second stage of compensation as proposed in [16]). One advantage of this scheme is that it may be possible to derive all of the required control information from frequency-dependent polarimetry data, which our wavelength-parallel polarimeter should be able to acquire within 1 ms.

In our work to date, we have focused on compensation of subpicosecond pulses, relevant for future ultra-high-speed time-division-multiplexed (TDM) systems. However, our scheme can be modified to work with narrowband wavelength-division-multiplexed (WDM) channels, and potentially multiple WDM channels may be compensated in a single setup. In this case, different WDM channels impinge on different subregions of the LCM. This reduces the number of pixels available for any single WDM channel; therefore, depending on the amount of PMD, the pixel resolutions and the overall frequency range spread across the LCM have to be adjusted. Fundamentally, the pulse-shaping system must provide spectral resolution

significantly finer than the information bandwidth of individual optical channels. For WDM channels at 10 or 40 Gb/s, this is a challenge for grating-based pulse shapers. To meet this challenge, one can consider pulse shapers based on high spectral dispersion devices such as virtually imaged phased arrays (VIPAs) [39]. In our group, we have recently demonstrated the use of VIPAs as demultiplexers with subgigahertz resolution at 50 GHz free spectral range compatible with dense WDM (DWDM) wavelength spacing [40]. We have also constructed a phase-only pulse shaper based on a VIPA spectral disperser, which we have utilized for tunable dispersion compensation for standard 10-Gb/s NRZ optical communications [41]. These results clearly demonstrate the possibility of pulse-shaping-based signal manipulations within the narrow bandwidths relevant for single WDM channels. Our group has also introduced a geometry that uses the combination of a VIPA and diffraction grating to achieve two-dimensional (2-D) separation of the optical spectrum, covering the entire lightwave C-band with approximately gigahertz resolution in a single setup [42], and has applied this 2-D setup for wavelength parallel polarization sensing [43]. Building on these results, it may be possible to realize 2-D pulse shaper setups incorporating 2-D LCM arrays, in which independent PMD compensation of individual WDM channels is achieved in parallel, with high fidelity and all-order capability for each channel.

Finally, it should also be possible to run our PMD compensator backwards to use it as a programmable all-order PMD emulator. In this case, the input to the system would be an undistorted pulse; the pulse shapers could be programmed to generate programmable spectral SOP and phase variations that mimic PMD. Further research may be needed to determine the appropriate control settings for this emulation concept.

ACKNOWLEDGMENT

The authors thank X. Wang, D. Leaird, L. Xu, and R. Nelson for their contributions.

REFERENCES

[1] H. Kogelnik, R. M. Jopson, and L. E. Nelson, "Polarization mode dispersion," in *Optical Fiber Telecommunications IV B—Systems and Impairments*, I. P. Kaminow and T. Li, Eds. San Diego, CA: Academic, 2002.

[2] P. Ciprut, B. Gisin, N. Gisin, R. Pass, J. P. Von der Weid, F. Prieto, and C. W. Zimmer, "Second-order polarization mode dispersion: Impact on analog and digital transmissions," *J. Lightw. Technol.*, vol. 16, no. 5, pp. 757–771, May 1998.

[3] C. Francia, F. Bruyère, D. Penninckx, and M. Chbat, "PMD second-order effects on pulse propagation in single-mode optical fibers," *IEEE Photon. Technol. Lett.*, vol. 10, no. 12, pp. 1739–1741, Dec. 1998.

[4] H. Bülow, "System outage probability due to first- and second-order PMD," *IEEE Photon. Technol. Lett.*, vol. 10, no. 5, pp. 696–698, May 1998.

[5] G. J. Foschini, R. M. Jopson, L. E. Nelson, and H. Kogelnik, "The statistics of PMD-induced chromatic fiber dispersion," *J. Lightw. Technol.*, vol. 17, no. 9, pp. 1560–1565, Sep. 1999.

[6] Q. Yu, L.-S. Yan, Y. Xie, M. Hauer, and A. E. Willner, "Higher order polarization mode dispersion compensation using a fixed time delay followed by a variable time delay," *IEEE Photon. Technol. Lett.*, vol. 13, no. 8, pp. 863–865, Aug. 2001.

[7] P. B. Phua and H. A. Haus, "Deterministic to first- and second-order PMD compensation," *IEEE Photon. Technol. Lett.*, vol. 14, no. 9, pp. 1270–1272, Sep. 2002.

[8] K. Ikeda, "PMD compensator with second-order PMD mitigation using mode-coupled fixed delay," *IEEE Photon. Technol. Lett.*, vol. 16, no. 1, pp. 105–108, Jan. 2004.

[9] F. Heismann, "Improved optical compensator for first- and second-order polarization-mode dispersion," *IEEE Photon. Technol. Lett.*, vol. 17, no. 5, pp. 1016–1018, May 2005.

[10] X. Zhang, L. Xi, L. Yu, G. Zhou, Y. Shen, J. Zhang, N. Zhang, B. Wu, T. Yuan, L. Chen, H. Zhang, M. Yao, and B. Yang, "Two-stage adaptive PMD compensation in 40 Gb/s OTDM optical communication system using PSO algorithm," *Opt. Quantum Electron.*, vol. 36, no. 12, pp. 1089–1104, Sep. 2004.

[11] G. Ouyang, A. Eyal, and A. Yariv, "An optimal feedforward design for complete PMD compensation up to the second order," *J. Lightw. Technol.*, vol. 22, no. 8, pp. 1844–1847, Aug. 2004.

[12] H. Miao and C. Yang, "Feed-forward polarization-mode dispersion compensation with four fixed differential group delay elements," *IEEE Photon. Technol. Lett.*, vol. 16, no. 4, pp. 1056–1058, Apr. 2004.

[13] S. Kim, "Schemes for complete compensation for polarization mode dispersion up to second order," *Opt. Lett.*, vol. 27, no. 8, pp. 577–579, Apr. 2002.

[14] M. Boroditsky, K. Cornick, C. Antonelli, M. Brodsky, D. S. Dods, N. J. Frigo, and P. Magill, "Comparison of system penalties from first- and multiorder polarization-mode dispersion," *IEEE Photon. Technol. Lett.*, vol. 17, no. 8, pp. 1650–1652, Aug. 2005.

[15] R. Noe, D. Sandel, M. Yoshida-Dierolf, S. Hinz, V. Mirvoda, A. Schopflin, C. Gungener, E. Gottwald, C. Scheerer, G. Fischer, T. Weyrauch, and W. Haase, "Polarization mode dispersion compensation at 10, 20, and 40 Gb/s with various optical equalizers," *J. Lightw. Technol.*, vol. 17, no. 9, pp. 1602–1616, Sep. 1999.

[16] P. B. Phua, H. A. Haus, and E. P. Ippen, "All-frequency PMD compensator in feedforward scheme," *J. Lightw. Technol.*, vol. 22, no. 5, pp. 1280–1289, May 2004.

[17] P. B. Phua and E. P. Ippen, "A deterministic broad-band polarization-dependent loss compensator," *J. Lightw. Technol.*, vol. 23, no. 2, pp. 771–780, Feb. 2005.

[18] C. K. Madsen, M. Capuzzo, E. J. Laskowski, E. Chen, L. Gomez, A. Griffin, A. Wong-Foy, S. Chandrasekhar, L. Stulz, and L. Buhl, "Versatile integrated PMD emulation and compensation elements," *J. Lightw. Technol.*, vol. 22, no. 4, pp. 1041–1050, Apr. 2004.

[19] A. M. Weiner, "Femtosecond pulse shaping using spatial light modulators," *Rev. Sci. Instrum.*, vol. 71, no. 5, pp. 1929–1960, May 2000.

[20] M. M. Wefers and A. K. Nelson, "Generation of high-fidelity programmable ultrafast optical waveforms," *Opt. Lett.*, vol. 20, no. 9, pp. 1047–1049, May 1995.

[21] M. Akbulut, R. Nelson, A. M. Weiner, P. Cronin, and P. J. Miller, "Broadband polarization correction with programmable liquid-crystal modulator arrays," *Opt. Lett.*, vol. 29, no. 10, pp. 1129–1131, May 2004.

[22] T. Brixner and G. Gerber, "Femtosecond polarization pulse shaping," *Opt. Lett.*, vol. 26, no. 8, pp. 557–559, Apr. 2001.

[23] M. Akbulut, A. M. Weiner, and P. J. Miller, "Wideband all-order PMD compensation via pulse shaping," *Opt. Lett.*, vol. 30, no. 20, pp. 2691–2693, Oct. 2005.

[24] M. Akbulut, L. Xu, A. M. Weiner, and P. J. Miller, "Wideband all order PMD compensation via pulse shaping," in *Proc. Optical Fiber Communications Conf.*, Mar. 2005, vol. 6, p. PDP7.

[25] A. M. Weiner, "Methods and systems for polarization control and polarization mode dispersion compensation for wideband optical signals," U.S. Patent 20020060760, May 23, 2002.

[26] Z. Zhuang, S. Suh, and J. S. Patel, "Polarization controller using nematic liquid crystals," *Opt. Lett.*, vol. 24, no. 10, pp. 694–696, May 1999.

[27] S. Särkimukka, A. Djjpsjöbacka, A. Gavler, and G. Jacobsen, "Mitigation of polarization-mode dispersion in optical multichannel systems," *J. Lightw. Technol.*, vol. 18, no. 10, pp. 1374–1380, Oct. 2000.

[28] C. Dorrer and F. Salin, "Phase amplitude coupling in spectral phase modulation," *IEEE J. Sel. Topics Quantum Electron.*, vol. 4, no. 2, pp. 342–345, Mar./Apr. 1998.

[29] R. N. Thurston, J. P. Heritage, A. M. Weiner, and W. J. Tomlinson, "Analysis of picosecond pulse shape synthesis by spectral masking in a grating pulse compressor," *IEEE J. Quantum Electron.*, vol. QE-22, no. 5, pp. 682–696, May 1986.

[30] A. M. Weiner, D. E. Leaird, J. S. Patel, and J. R. Wullert, II, "Programmable shaping of femtosecond optical pulses by use of 128-element liquid crystal phase modulator," *IEEE J. Quantum Electron.*, vol. 28, no. 4, pp. 908–920, Apr. 1992.

[31] H. Wang, Z. Zheng, D. E. Leaird, A. M. Weiner, T. A. Dorschner, J. J. Fijol, L. J. Friedman, H. Q. Nguyen, and L. A. Palmaccio, "20-fs pulse shaping with a 512-element phase-only liquid crystal modulator,"

IEEE J. Sel. Topics Quantum Electron., vol. 7, no. 4, pp. 718–727, Jul./Sep. 2001.
[32] H. Chen, R. M. Jopson, and H. Kogelnik, "On the bandwidth of higher-order polarization-mode dispersion: The Taylor series expansion," *Opt. Express*, vol. 11, no. 11, pp. 1270–1282, Jun. 2003.
[33] Z. Jiang, D. S. Seo, D. E. Leaird, and A. M. Weiner, "Spectral line-by-line pulse shaping," *Opt. Lett.*, vol. 30, no. 12, pp. 1557–1559, Jun. 2005.
[34] X. Wang and A. M. Weiner, "Fast wavelength-parallel polarimeter for broadband optical networks," *Opt. Lett.*, vol. 29, no. 9, pp. 923–925, May 2004.
[35] R. Trebino, *Frequency-Resolved Optical Gating: The Measurement of Ultrashort Laser Pulses*. Boston, MA: Kluwer, 2000.
[36] J. Peatross and A. Rundquist, "Temporal decorrelation of short laser pulses," *J. Opt. Soc. Amer. B, Opt. Phys.*, vol. 15, no. 1, pp. 216–222, Jan. 1998.
[37] A. Rundquist, A. Efimov, and D. H. Reitze, "Pulse shaping with the Gerchberg–Saxton algorithm," *J. Opt. Soc. Amer. B, Opt. Phys.*, vol. 19, no. 10, pp. 2468–2478, Oct. 2002.
[38] P. F. McManamon, T. A. Dorschner, D. L. Corkum, L. J. Friedman, D. S. Hobbs, M. Holz, S. Liberman, H. Q. Nguyen, D. P. Resler, R. C. Sharp, and E. A. Watson, "Optical phased array technology," *Proc. IEEE*, vol. 84, no. 2, pp. 268–298, Feb. 1996.
[39] M. Shirasaki, "Large angular dispersion by a virtually imaged phased array and its application to a wavelength demultiplexer," *Opt. Lett.*, vol. 21, no. 5, pp. 366–368, Mar. 1996.
[40] S. Xiao and A. M. Weiner, "An eight-channel hyperfine wavelength demultiplexer using a virtually-imaged phased-array (VIPA)," *IEEE Photon. Technol. Lett.*, vol. 17, no. 2, pp. 372–374, Feb. 2005.
[41] G.-H. Lee, S. Xiao, and A. M. Weiner, "Programmable, polarization-independent, and DWDM-capable chromatic dispersion compensator using a virtually-imaged phased-array and spatial light modulator," in *Proc. Optical Fiber Communications Conf.*, 2006.
[42] S. Xiao and A. M. Weiner, "2-D wavelength demultiplexer with potential for $\geq$1000 channels in the C-band," *Opt. Express*, vol. 12, no. 13, pp. 2895–2902, Jun. 2004.
[43] S. X. Wang, S. Xiao, and A. M. Weiner, "High resolution and high speed wavelength-parallel polarization sensor for dense WDM systems," in *Proc. Optical Fiber Communications Conf.*, Mar. 2005, vol. 4.

Mehmetcan Akbulut (S'97–M'05) received the M.S. and Ph.D. degrees in electrical and computer engineering from Purdue University, West, Lafayette, IN, in 2001 and 2005, respectively. His research focused on "all-order polarization mode dispersion compensation" using pulse-shaping technology.

His earlier work included ultra-high-speed light-emitting devices (LEDs) for short-haul optical networks and GaAs semiconductor detector structures. He is currently with Pritel Inc., Naperville, IL, developing state-of-the-art fiber lasers and amplifiers for telecommunications research.

Andrew M. Weiner (S'84–M'84–SM'91–F'95) received the Sc.D. degree in electrical engineering from Massachusetts Institute of Technology (MIT), Cambridge, in 1984.

From 1979 through 1984, he was a Fannie and John Hertz Foundation Graduate Fellow at MIT. Upon graduation, he joined Bellcore, first as member of Technical Staff and later as Manager of Ultrafast Optics and Optical Signal Processing Research. He moved to Purdue University, West, Lafayette, IN, in 1992 and is currently the Scifres Distinguished Professor of Electrical and Computer Engineering. From 1997 to 2003, he served as the ECE Director of Graduate Admissions. His research focuses on ultrafast optical signal processing and high-speed optical communications. He is especially well known for pioneering the field of femtosecond pulse shaping, which enables generation of nearly arbitrary ultrafast optical waveforms according to user specification. He has published five book chapters and over 160 journal articles and is a coeditor of one book. He has been the author or a coauthor of over 300 conference papers, including approximately 80 conference invited talks, and has presented over 70 additional invited seminars at university, industry, and government organizations. He holds eight U.S. patents.

Prof. Weiner is a Fellow of the Optical Society of America (OSA). He has received numerous awards for his research, including the Hertz Foundation Doctoral Thesis Prize (1984), the Adolph Lomb Medal of the Optical Society of America (1990), awarded for pioneering contributions to the field of optics made before the age of 30, the Curtis McGraw Research Award of the American Society of Engineering Education (1997), the International Commission on Optics Prize (1997), the IEEE LEOS William Streifer Scientific Achievement Award (1999), the Alexander von Humboldt Foundation Research Award for Senior U.S. Scientists (2000), and the inaugural Research Excellence Award from the Schools of Engineering at Purdue (2003). He has served on or chaired numerous research review panels, professional society award committees, and conference program committees. From 1988 to 1989, he served as an IEEE Lasers and Electro-optics Society (LEOS) Distinguished Lecturer. He has served as Chair or Co-Chair of the Conference on Lasers and Electro-Optics, the Gordon Conference on Nonlinear Optics and Lasers, and the International Conference on Ultrafast Phenomena. He has also served as Associate Editor for IEEE JOURNAL OF QUANTUM ELECTRONICS, IEEE PHOTONICS TECHNOLOGY LETTERS, and *Optics Letters*. He served as an Elected Member of the Board of Governors of IEEE LEOS from 1997 to 1999 and as Secretary/Treasurer of IEEE LEOS from 2000 to 2002. From 2002 to 2005, he was a Vice-President (representing IEEE LEOS) of the International Commission on Optics (ICO).

Peter J. Miller received the B.A. and M.Sc. degrees.

He was the founder of CRI, Inc., where he has developed liquid crystal tunable filters and spatial light modulators for scientific research and telecommunications use. He holds 19 U.S. patents and helped develop products that won three R&D 100 awards. His interests include spectral imaging, polarimetry, colorimetry, and liquid crystal devices